Journal of Structural Biology 178 (2012) 76–83

Contents lists available at SciVerse ScienceDirect

Journal of Structural Biology

journal homepage: www.elsevier.com/locate/yjsbi

Reconstructing adhesion structures in tissues by cryo-electron tomography of vitrified frozen sections

Melanie Bokstad [a], Helena Sabanay [b], Idit Dahan [a], Benjamin Geiger [b,*], Ohad Medalia [a,c,*]

[a] Department of Life Sciences, Ben-Gurion University of the Negev, BeerSheva 84105, Israel
[b] Department of Molecular Cell Biology, Weizmann Institute of Science, Rehovot 76100, Israel
[c] Department of Biochemistry, University of Zurich, 8057 Zurich, Switzerland

ARTICLE INFO

Article history:
Available online 7 November 2011

Keywords:
Cell adhesion
Cryo-sectioning
Cryo-electron tomography
Refrozen tissue
Vitrified frozen section (VFS)
Tokuyasu technique
Sectioning
Smooth muscle

ABSTRACT

Cryo-electron tomography enables three-dimensional insights into the macromolecular architecture of cells in a close-to-life state. However, it is limited to thin specimens, <1.0 μm in thickness, typically restricted to the peripheral areas of intact eukaryotic cells. Analysis of tissue ultrastructure, on the other hand, requires physical sectioning approaches, preferably cryo-sectioning, following which electron tomography (ET) may be performed. Nevertheless, cryo-electron microscopy of vitrified sections is a demanding technique and typically cannot be used to examine thick sections, >80–100 nm, due to surface crevasses. Here, we explore the potential use of cryo-ET of vitrified frozen sections (VFSs) for imaging cell adhesions in chicken smooth muscle and mouse epithelial tissues. By investigating 300–400 nm thick sections, which are collected on the EM grid and re-vitrified, we resolved fine 3D structural details of the membrane-associated dense plaques and flanking caveoli in smooth muscle tissue, and desmosomal adhesions in stratified epithelium. Technically, this method offers a simple approach for reconstructing thick volumes of hydrated frozen sections.

1. Introduction

A realistic three-dimensional (3D) visualization of cells and tissues at molecular resolution, is critical to our understanding of physiological processes. Conventionally, electron microscopy is used for looking into cells; however, traditional sample preparation methodologies involve sample dehydration and heavy-metal staining, enabling the retrieval of rich morphological information, yet subject to potential perturbations, due to the dehydration and chemical staining steps (Al-Amoudi et al., 2004; Kellenberger and Kistler, 1979; Mollenhauer, 1993; Norlen et al., 2009; Steere, 1957). Furthermore, conventional electron microscopy essentially derives 2D projections of the sample, in which features are superimposed upon one another in the direction of the electron beam. This approach can provide good contrast and overall structural preservation, but lacks the 3D element (Sabanay et al., 1991).

The three-dimensionality of a sample can, however, be retrieved in a close-to-life state by means of cryo-electron tomography (cryo-ET), enabling the acquisition of information needed for the detailed reconstruction of the 3D structure of unperturbed cells, the pericellular space, and intracellular organelles (Lucic et al., 2008; Mader et al., 2010; Yahav et al., 2011). Nevertheless, cryo-ET is limited by the sample thickness to <1.0 μm-thick samples (Medalia et al., 2002). Therefore, physical cryo-sectioning approaches are needed to study thick cellular and tissue specimens, followed by examination of the sections in the frozen-hydrated state. Over 40 years ago, Christensen and McDowall (Christensen, 1971; McDowall et al., 1983) suggested that directly vitrified sections be examined; however, technical difficulties, mainly involving inadequate cryo-ultramicrotome systems such as, for example, knife quality, prevented the use of this approach until a decade ago, when an improved cryo-ultramicrotome set-up, enabling successful vitrified sectioning, was developed (Bouchet-Marquis and Hoenger, 2011; Hsieh et al., 2002). Since that time, cryo-electron microscopy of vitrified sections (CEMOVIS) has become a powerful tool for investigating the fine structural features of cellular compartments (Sader et al., 2009).

A major step forward in tissue imaging was taken, when CEMOVIS was coupled with electron tomography of vitreous sections. In combination, these techniques proved to be successful for obtaining high quality structural data in a close-to-native approach without dehydration, fixation and staining of the specimen (Al-Amoudi et al., 2004, 2007; Gruska et al., 2008; Hsieh et al., 2006). However, section thickness remains a major limitation in CEMOVIS. It was further shown that increasing section thickness to 150 nm may

* Corresponding authors. Address: Department of Biochemistry, University of Zurich, 8057 Zurich, Switzerland (O. Medalia).
E-mail addresses: benny.geiger@weizmann.ac.il (B. Geiger), omedalia@bioc.uzh.ch (O. Medalia).

1047-8477/$ - see front matter © 2011 Elsevier Inc. All rights reserved.
doi:10.1016/j.jsb.2011.10.013

enable resolution of structural details within the range of 6–10 nm (Gruska et al., 2008), although sections thicker than 100 nm would frequently contain crevasses (Al-Amoudi et al., 2005) [i.e., local section fractures oriented parallel to the sectioning direction, and penetrating the section from one side (Han et al., 2008)]. Thus, CEMOVIS enables a close-to-native view of tissues (Al-Amoudi et al., 2007, 2011; Bouchet-Marquis and Hoenger, 2011); yet is prone to artifacts such as compression, chatter, crevasses and knife marks, as well as breaks caused by section handling (Al-Amoudi et al., 2005).

Here, we present a strategy combining cryo-ET with the vitrified frozen sections (VFSs) approach (Sabanay et al., 1991). VFS combines the classical Tokuyasu method (Tokuyasu, 1973) with re-vitrification of the sections associated with the EM grid, circumventing sample dehydration and heavy metal staining. Examination of the sections using cryo-ET enabled us to acquire unprecedented views of cell adhesions, of smooth muscle cells and desmosomes, of chicken gizzard adhesion sites, and of dermis desmosomes.

2. Results

Smooth muscle from chicken gizzard has been used for several decades as a primary source of cytoskeletal proteins, as well as an excellent model for studying integrin-mediated membrane–cytoskeleton interactions. Moreover, the contractile machinery of smooth muscle has been subjected to a wide variety of sample preparation procedures, including 'conventional' plastic sections (Chang et al., 1994), frozen sections (Geiger et al., 1980, 1981), freeze fracture, and deep etching (Somlyo, 1985). Live-cell imaging techniques, combined with tomography, have also been applied to analyze adhesion structures (Small and Kaverina, 2003; Urban et al., 2010). Accordingly, we chose this tissue as one of the primary systems for investigating the potential use of our VFS for cryo-ET. In addition, we examined stratified epithelial tissue from mouse tongue. Epidermal tissue has been extensively used for studies of desmosomes and their components, by various means (Frank et al., 2001; Garrod, 1993; Garrod et al., 2002; Giudice et al., 1984; Koulu et al., 1984; Runswick et al., 2001; Steinberg et al., 1987). The process, from tissue fixation to acquisition of 3D volumes, is outlined in Fig. 1.

2.1. Visualizing dense plaques and the associated cytoskeleton in gizzard smooth muscle

Using the above approach, we produced 300–400 nm-thick frozen hydrated sections, and acquired a cryo-tomographic tilt series of their dense plaques. A low-magnification projection of a hydrated section is shown in Fig. 2A, demonstrating the overall structure of the tissue, and the typical contrast of the cryo images. Based on such a view, we zoomed into an adhesion region for tomographic analysis (Fig. 2A, area framed in black). Looking at x–y tomographic slices, 9 nm in thickness, made it possible to identify typical structures such as dense plaques (DP), mitochondria (Mi), caveolae (arrows) as well as myofilaments (arrowhead), that all of which are mostly aligned along the major cell axis (Fig. 2B). Examination of the pericellular connective tissue revealed thick extracellular fibers, presumably collagen (arrow), which are often clustered together, and run along the sarcolemma (Fig. 2C).

Zooming in on the adhesion dense plaques (Fig. 2C), the actin–membrane interface of these integrin adhesions was apparent, in unprecedented detail. Fig. 2D shows part of the DP from Fig. 2C at higher magnification. Filaments with a diameter of ~7 nm (most likely, actin filaments), are seen, spanning the entire thickness of the electron-dense plaque, all the way to the membrane (Fig 2D, arrowheads) (Hanson, 1963; Shao et al., 2000; Shi et al., 2001). Interestingly, unlike the uniform alignment of the filaments throughout the cytoplasm, the filaments within the plaque display variable orientations (see below). In addition, ring-like molecular complexes with a diameter of 20–25 nm are frequently detected along the membrane, within DPs (Fig. 2D, black boxes). A group of particles (pictured in Fig. 2E) appears quite similar to those of the focal adhesion-related particles described by Patla et al. (2010). This finding suggests that the adhesion-related particles

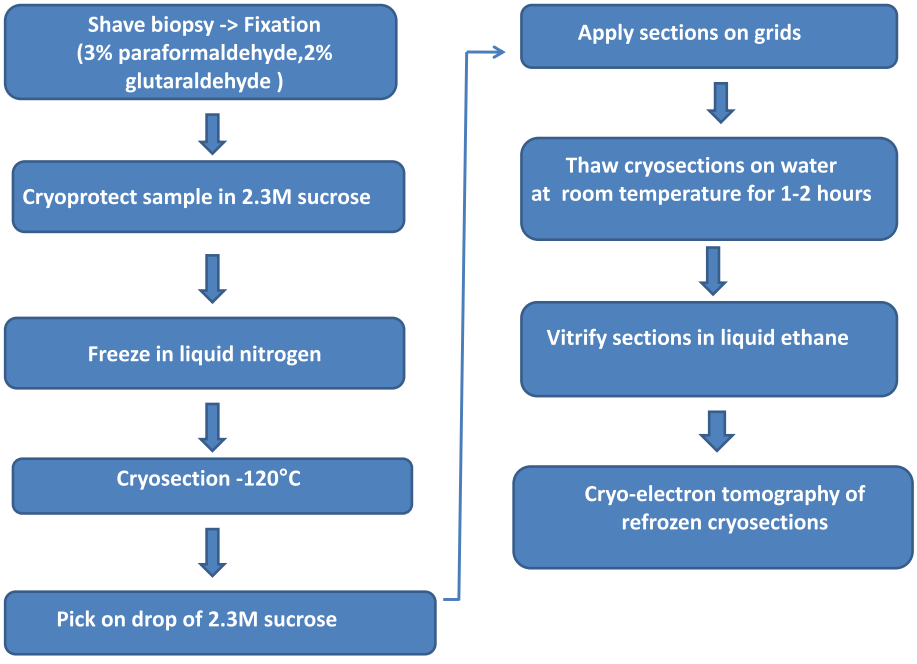

Fig.1. The experimental steps for VFS followed by cryo-ET. Tissue samples are fixed and incubated in 2.3 M sucrose, prior to freezing in liquid nitrogen. Next, 300–400 nm-thick cryo-sections are cut and transferred with a sucrose droplet to EM grids, at room temperature. After the thawing step, the sections are washed in water for 2 h, then vitrified and analyzed by cryo-ET (see Section 4).

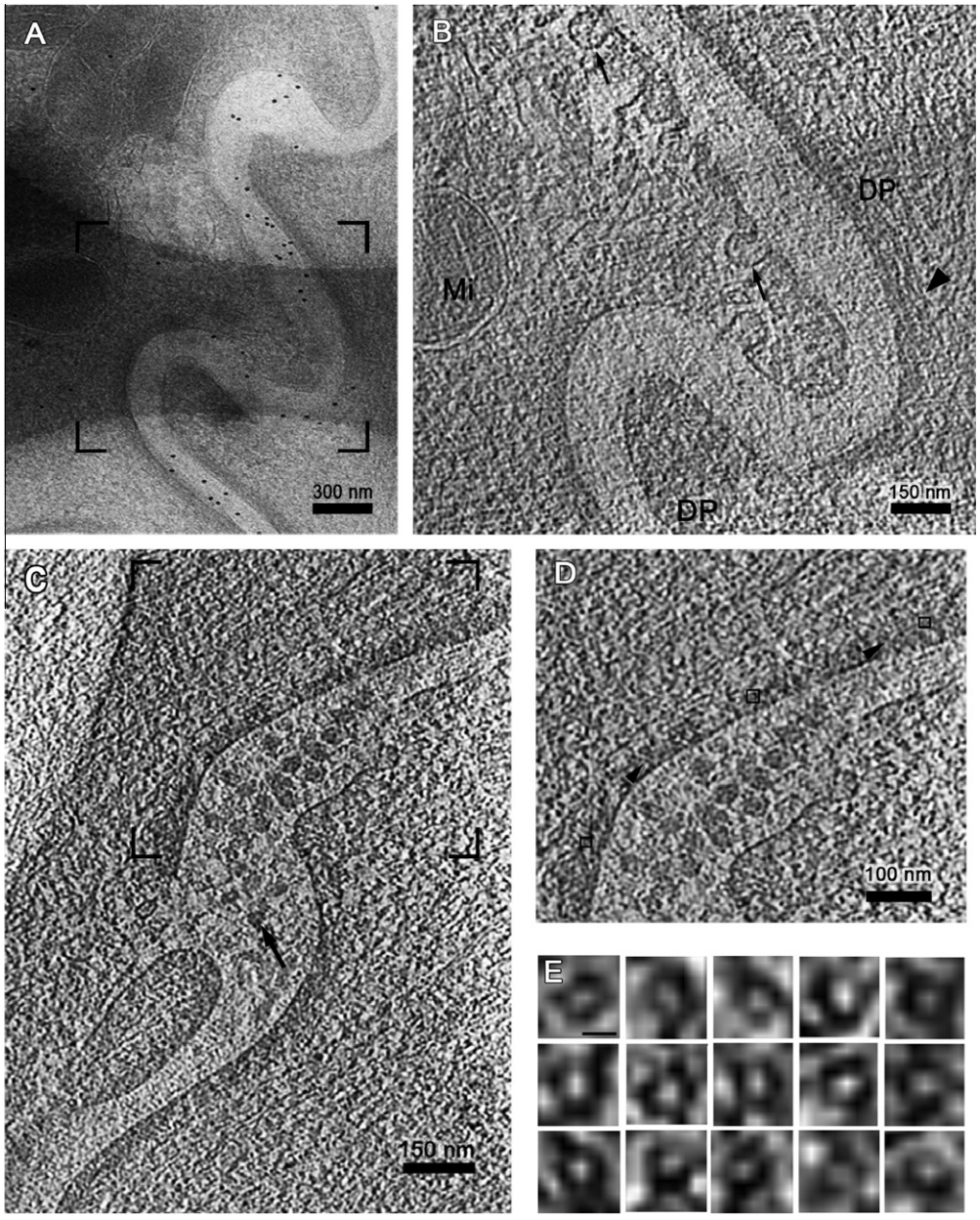

Fig.2. Vitrified sections from chicken gizzard, analyzed by cryo ET. (A) A low magnification cryo-EM image of a hydrated section of chicken gizzard smooth muscle, 300 nm in thickness, shows a typical region used for data analysis of adhesion sites. (B) A tomographic slice, 9 nm in thickness, from the region shown in (A), (outlined in black). Dense plaques (DP), caveolar (marked with arrows), mitochondria (Mi) and filaments (arrowhead) of a gizzard junction section. (C) A tomographic slice, 9 nm in thickness, from an additional section, showing collagen fibers in the extracellular space (arrow). (D) Higher magnification of the region shown in (C), outlined in black, showing cytoplasmic actin filaments, as well as filaments attaching to the cytoplasmic plaques (black arrowheads) and molecular assemblies adjacent to the membrane (black squares), resembling adhesion-related particles seen in focal adhesions (Patla et al., 2010). (E) A set of molecular complexes resembling the adhesion-related particles. Scale bar: 12 nm.

may be found in many forms at integrin-mediated adhesion sites, both in culture and *in vivo*.

2.2. Actin filaments insert themselves into dense plaques in multiple directions

In the course of this work, we reconstructed over forty volumes of adhesion sites from chicken smooth muscle tissue. Fig. 3A and B shows successive slices through another tomographic volume. In order to gain deeper insights into the cytoskeletal network at these integrin adhesion sites, we produced a surface rendering view from the ~300 nm-thick section. These data clearly show the 3D organization of the contractile cytoskeletal network, the DP, the caveolea and the extracellular connective tissue, in stereo views (Fig. 3C). We conclude that VFS enables detection of actin filaments and all other components of the smooth muscle section, in a hydrated state. This approach enables the visualization of the internal structure of the DP of the smooth muscle cells, providing information about the typical thickness of the structure (88.5 ± 2.4 nm), the filament organization within the plaque, and the presence of adhesion-related particles in the interface between the actin filaments and the membrane.

2.3. Structural preservation of desmosomes in stratified epithelial tissue using VFS

To further examine the quality of structural preservation of cell adhesion structures, we applied VFS in a manner similar to that

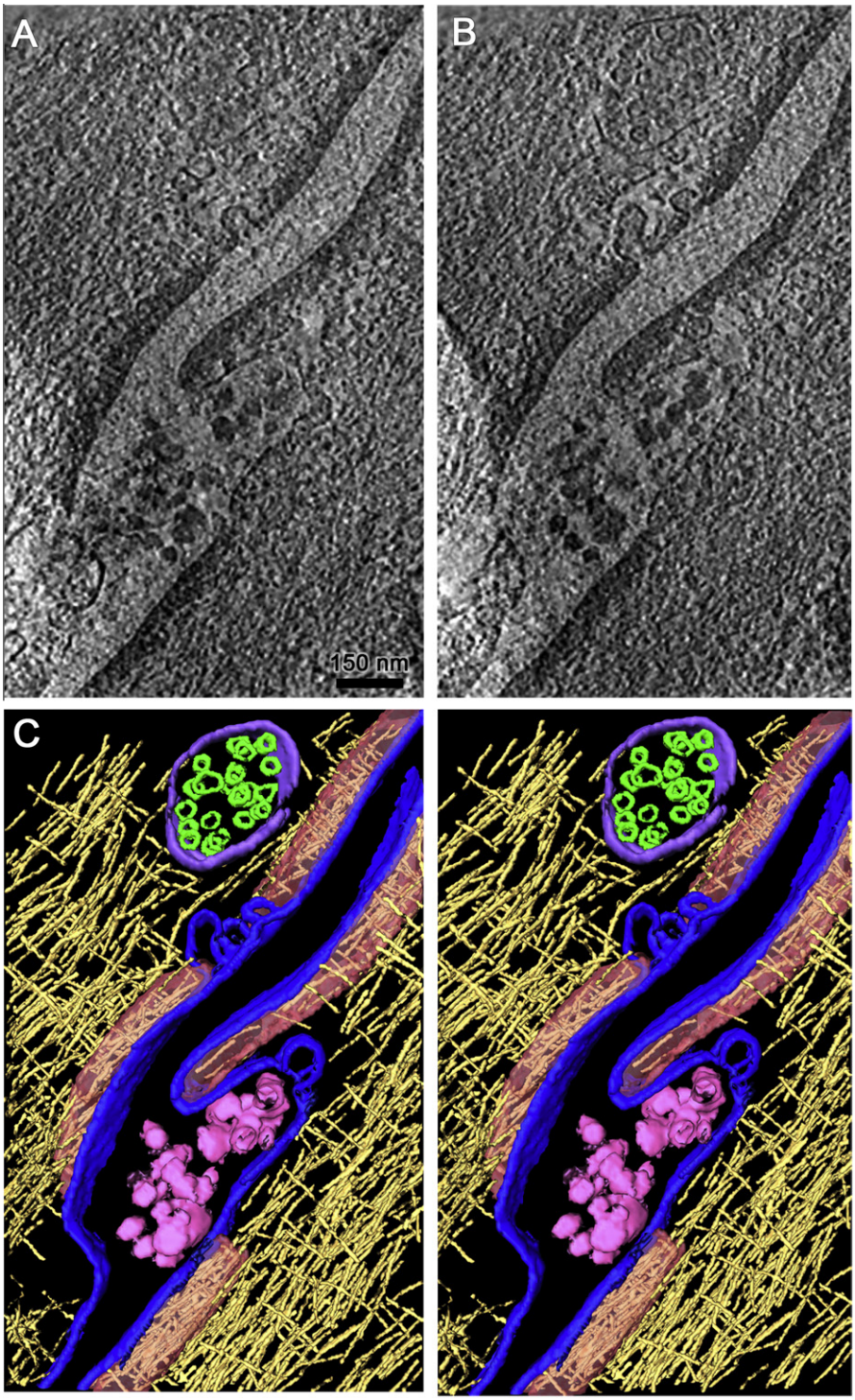

Fig.3. Three-dimensional view of the chicken gizzard cell periphery. (A and B) Successive tomographic slices, 9 nm in thickness, through a reconstructed volume of chicken gizzard smooth muscle tissue (C) A surface-rendered view of an adhesion junction, shown in stereo. Membrane (blue), dense plaques (transparent red), actin (yellow), collagen (light pink), multi-vesicular vesicle (purple) and vesicles inside the multi-vesicular compartment (green) were segmented.

described above, to mouse stratified epithelial tissues from mouse tongue. Epithelial tissues are enriched with different types of cell–cell junctions, including cytokeratin-associated desmosomes. These adhesions play an important role in tissue morphogenesis, and display a characteristic laminated structure. The fine structure of desmosomes, including the identity and localization of their diverse components, has been well-documented (Franke et al., 1987; Garrod, 1993; Garrod et al., 2002; Giudice et al., 1984; Koulu et al., 1984; Steinberg et al., 1987), enabling us to compare the structural information attained with the VFS-cryoET approach, to that obtained by other methods (Al-Amoudi et al., 2007; Delva et al., 2009; Franke et al., 1987; Garrod and Chidgey, 2008; Giudice et al., 1984; Koulu et al., 1984; Steinberg et al., 1987). Here, we analyzed mouse epithelial tissues, specifically focusing on desmosome structures. We were able to detect fine details which were comparable to previous findings (Al-Amoudi et al., 2007; Franke

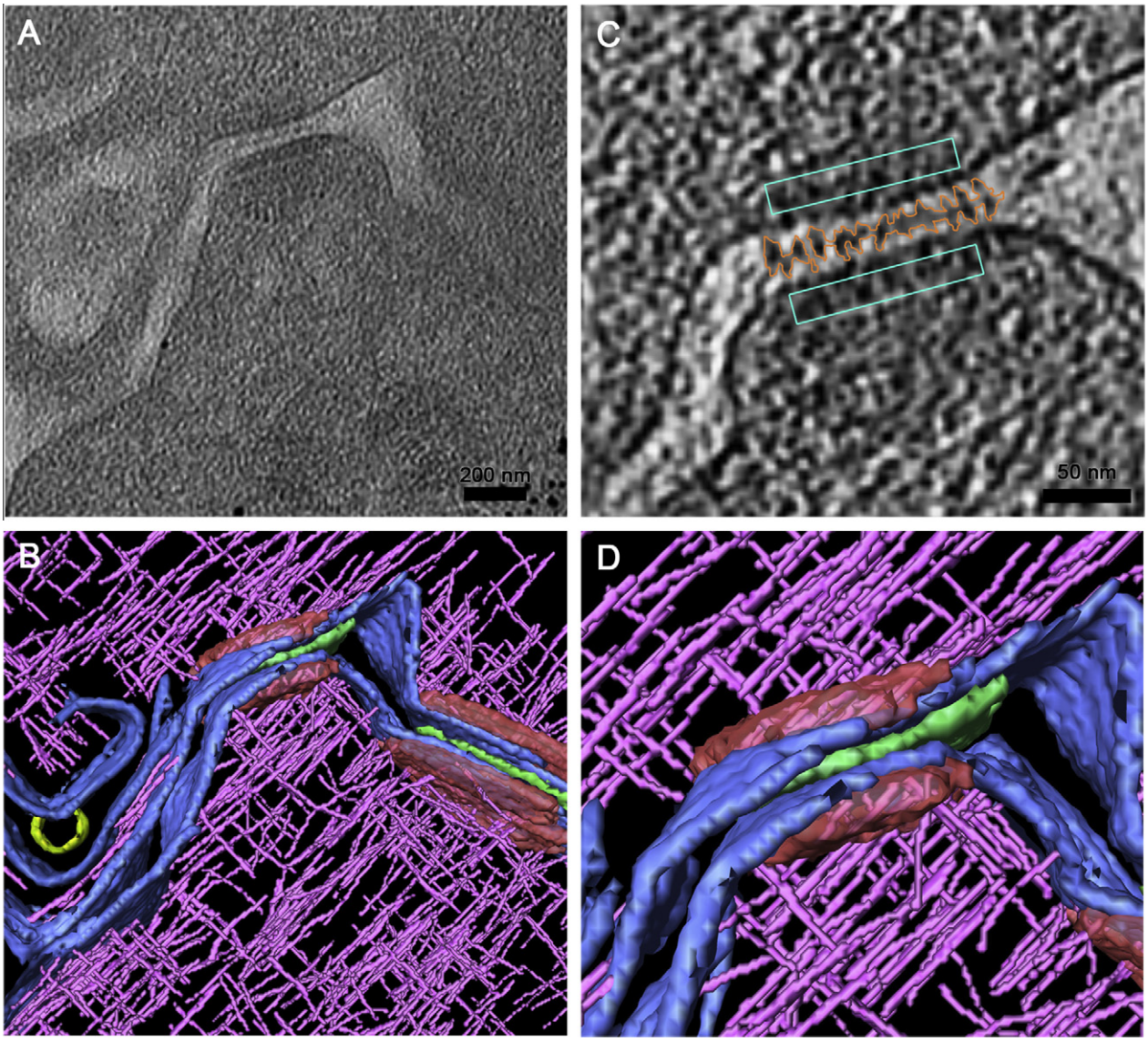

Fig.4. Epithelial mouse tongue tissue analyzed by cryo-ET. (A) A tomographic slice, 6 nm in thickness, from a 300 nm-thick section, showing a desmosomal region. (B) A surface-rendered view of the region of the desmosome shown in (A). Membrane (blue), keratin (pink), dense plaques (transparent red), vesicle in the extracellular space (transparent green) and electron dense midline of the desmosome (green) were segmented. (C) A close-up view of the desmosome. The orange density layer-line illustrates the characteristic rod-like structures, as well as the dense midline. The intracellular blue squares indicate the dense protein mesh of the cytoplasmic surface of the desmosome. (D) Higher magnification view of the desmosome in (C) is shown as a surface-rendered view. A substantial number of keratin filaments are shown interacting with the cytoplasmic plaque of desmosomes.

et al., 1987; Garrod, 1993; Garrod et al., 2002; Runswick et al., 2001; Steinberg et al., 1987). An overview projection and a tomographic slice through a desmosome are shown in Fig. 4A and C, respectively. In the projection image, we observed the characteristic phenotype of the dense midline of desmosomes between the two membranes of different cells (Garrod and Chidgey, 2008; Garrod et al., 2002). The desmosomal cadherins, e.g. desmocollins and desmogleins, appear straight, and are densely packed along the intercellular interface, forming quasi-periodic densities between the membrane and the midline (Fig. 4C, orange). Furthermore, the cytoplasmic surface of the intercellular junction and its complicated arrangement of molecules and interactions, which link the ECM of desmosomal cadherins to the cytoskeletal intermediate filaments of the cell, were detected (Fig. 4C).

Immunological tools for localizing specific desmosomal components have been employed since the mid-1980s by the Franke and Steinberg laboratories, to locate specific desmosomal components (Franke et al., 1987; Giudice et al., 1984; Koulu et al., 1984; Steinberg et al., 1987). These findings, together with prior work, conducted primarily by means of electron microscopy (Garrod and Chidgey, 2008), revealed the desmosomal structure and its interacting components. The structure displays the characteristic dense midline, with cross-bridges extending from the midline to the plasma membrane. It is believed that the midline is indicative of a highly organized arrangement of the extracellular domains of the desmosomal cadherins. This information stands in accordance with recent investigations by Al-Amoudi et al., in which the three-dimensional reconstructions of desmosomes reveal a regular array of densities at intervals along the midline, with a curved shape resembling the X-ray structure of C-cadherin, a representative 'classical' cadherin. (Al-Amoudi et al., 2007).

The desmosome may be divided into three morphologically distinct zones: the extracellular core region (desmoglea), the outer dense plaque (ODP), and the inner dense plaque (IDP) on the intracellular side. Our data indicate that keratin intermediate filaments enter the dense plaque (Fig. 4), and are believed to bind to

desmoplakin within the IDP, which anchors the filaments to the plasma membrane (Delva et al., 2009). Thus, the structures we observe confirm previous findings in the desmosomal field (Al-Amoudi et al., 2007, 2011; Delva et al., 2009; Garrod and Chidgey, 2008; Garrod, 1993; Garrod et al., 2002). In the surface-rendered view (Fig. 4B and D), the cytokeratin densities (pink) and their interactions with the desmosomal plaques can be detected, demonstrating the density of filaments associated with these essential adhesion structures. Furthermore, the distances between the membranes in desmosome of adhering cells were measured in 22 reconstructed desmosomes, and averaged 36 ± 2.5 nm. This measurement suggests that structural deformation due to cutting forces is independent of sectioning directionality, and may thus provide additional evidence of the high quality of structure preservation.

3. Discussion

3.1. VFS: A simple approach to the production and examination of thick sections for cryo-ET

Our interest in the structure and function of adhesion structures created a strong motivation to develop optimal technologies for high-resolution examination of such structures, under minimal perturbation conditions. Based on the considerations mentioned above, we chose to study integrin-based adhesions and desmosomal junctions in the fully hydrated state, combining the preparation of frozen sections, retrieval of the sections on an EM grid, and their examination by cryo-ET. Due to the complexity of adhesion structures and their sheer size, thick hydrated sections are needed, in order to reconstruct their nano-architecture.

VFS provide a relative simple protocol for performing such experiments, producing relatively thick sections (300–400 nm) with satisfactory structural preservation of the tested tissues. The thickness of the sections enables the reconstruction of a 3D structure using cryo-ET. These features of the VFS-cryoET offer an advantage over the alternative CEMOVIS approach, which is based on keeping sections continuously frozen, but cannot provide meaningful 3D information on 300–400 nm thick sections. Thick sections are prone to artifacts, including crevasses, chatter and compression, commonly encountered in CEMOVIS (Al-Amoudi et al., 2005). In the VFS-cryoET approach, these artifacts are presumably circumvented, not only by the thickness of the section *per se*, but also by the thawing of the sections on the grid, prior to the vitrification process. Initially, this thawing step was a source of potential concern, due to the possibility that thawing and re-vitrification might affect the preservation of the tissue's ultrastructure. Nevertheless, results indicate that the structural preservation attained by the VFS-cryoET method is excellent, in line with our previous VFS-2D work (Sabanay et al., 1991). Part of this preservation of structural integrity is attributed to the use of sucrose infusion, in order to prevent damage to the tissue sample from freezing, and to the chemical fixation that prevents tissue destruction upon thawing (Tokuyasu, 1973). Indeed, the excellent structural preservation obtained by means of VFS depends on chemical fixation, and no sectioning artifacts are detected.

3.2. VFS reveals actin filament organization throughout the cytoplasm, and in the adhesion plaques of smooth muscle

Many studies have addressed the organization of actin filaments in smooth muscle tissue. Thin filaments of the contractile apparatus were previously shown to be uniformly aligned and densely packed in such tissue, cross-linked via "dense bodies" (i.e., dense adhesion plaques) distributed throughout the cytoplasm (Bond and Somlyo, 1982; North et al., 1994; Small and Gimona, 1998; Somlyo et al., 1983; Wolfenson et al., 2009). These actin filaments are also known to interact with the plasma membrane via dense plaques located at the cell periphery; yet the mode of this interaction remains unclear. Specifically, due to difficulties in resolving structural details in stained dehydrated samples, it was not known whether the sub-membrane plaque structure mediates the interaction of actin filaments with the sarcolemma, or whether the filaments extend through the plaque and reach the membrane.

As in other cells, actin is known to interact with the plasma membrane in chicken gizzard smooth muscle (Gabella, 1985; Gunst and Zhang, 2008). However, due to imaging limitations and the complexity of tissue adhesion structures, it is not clear if actin filaments directly interact with the plaque components or the membrane. Our study supports the notion that interactions between actin filaments and the dense adhesion plaque indeed, exists. Nevertheless, we cannot exclude the possibility that filamentous structures attach directly to the membrane domain, due to the limited resolution and the high density of the cytoplasmic plaque, shedding many details within the dense plaque. However, within the dense adhesion structures of chicken gizzard smooth muscle cells, we succeeded in identifying macromolecular complexes, similar in dimensions to the adhesion-related particles found in focal adhesions of fibroblast cells (Patla et al., 2010). This observation may indicate a general molecular composition and mechanical function of the integrin adhesion machinery.

3.3. Applying VFS and cryo-ET approaches to the study of desmosomes in stratified epidermal epithelium

Other adhesion structures, on which a rich structural literature exists, are desmosomal junctions, present primarily in epithelial tissues and cardiac muscle. These structures were of particular interest for us since recently, Al-Amoudi et al. provided detailed insights into the structure of desmosomes from human epithelial tissue, by means of CEMOVIS and cryo-ET (Al-Amoudi et al., 2007, 2011). Thus, coupled with our general interest in adhesion structures, we had an excellent opportunity to compare the two approaches. Accordingly, we used VFS to reconstruct thick volumes of mouse tongue tissue. Our data are in excellent agreement with the periodic, rod-like structures of the desmosomal cadherin network at the cytoplasmic surface of the desmosomes, as reconstructed following CEMOVIS. Our reconstruction indicated a relatively uniform intermembrane spacing of 36 nm, based on measurements performed on 22 desmosomes. This value is essentially indistinguishable from that obtained by CEMOVIS (35 nm) (Al-Amoudi et al., 2007). This result further suggests that the VFS methodology excels in preserving the structure of the biological samples studied. Other notable strengths of our VFS approach include an ability to follow the desmosome-associated fibers (mostly – cytokeratin fibers) into the plaque at different orientations, elucidating the fine structure of the cytoskeleton–membrane interactions at desmosomal adhesions.

In summary, we demonstrate here a simple and general methodology to produce frozen hydrated tissue sections, that can subsequently be studied by means of cry-electron tomography. Despite the use of chemical fixation, it seems that the structural preservation within the investigated tissues is satisfactory. VFS may be a method of choice to analyze hydrated 300–400 nm-thick sections of tissue. However, complementary, novel methodologies such as cryo-dual beam sectioning (Marko et al., 2007; Rigort et al., 2010) may provide the technical means to study thick hydrated section are to be accessible in the future.

4. Materials and methods

4.1. Sample preparation

Tissue from chicken gizzard smooth muscle and mouse epithelium from tongue (filiform papillae) were analyzed. Freshly dissected tissues were incubated in freshly prepared Karnovsky fixative. The tissue was dissected in the same fixative solution, and cut to the correct orientation. The tissue was fixed with Karnovsky fixative (3% paraformaldehyde, 2% glutaraldehyde 5 mM $CaCl_2$ in 100 mM cacodylate buffer, pH7.4) at room temperature, placed on a shaker for 4 h, and then placed at 4 °C overnight. The next day, the tissue was impregnated with 100 mM cacodylate buffer with 2.3 M sucrose, pH 7.4. The samples were then cut into small pieces and quick-frozen in liquid nitrogen. The sections were cut at minus 105 °C to thicknesses of 250–400 nm, using a Leica EM FC6 ultra cryo-microtome and transferred with a sucrose droplet to carbon-coated molybdenum grids. The grids were floated on double-distilled water in a Petri dish for approximately 2 h. For vitrification, grids were removed from the water. A 5 μl drop of bovine serum albumin (BSA)-coated 15 nm gold colloids in PBS was added to the EM grid, prior to blotting and freeze-plunging of the grids into liquid nitrogen-cooled ethane, before transferred to the electron microscope.

4.2. Data acquisition

Specimens were transferred under liquid N_2 temperature into 300 kV FEG polara transmission electron microscope (FEI, Eindhoven) equipped with a Gatan post-column GIF 2002 energy filter. Tilt series were acquired, covering an angular range of −60° to 60°; with a 2° tilt increments and a defocus of −6 μm, for the both the chicken gizzard samples and for the desmosomes. The magnification used was 18 K, and resulted in a pixel size of 0.82 nm at the specimen level.

4.3. Data analysis

Projection images (2048 × 2048 pixels) were aligned to a common origin, using 15-nm-sized fiducial gold markers, and reconstructed by means of weighted back-projection, as implemented by the TOM toolbox software package (Nickell et al., 2005). All tomograms were reconstructed with a binning factor, to yield a 1.64^3 nm^3 voxel size.

Surface-rendered visualizations were constructed, using the surface-rendering option in the AMIRA 5.3 software package (ZIB, Visage Imaging).

Acknowledgments

This study was supported by a grant from the German-Israeli Cooperation Project (DIP H.2.2) to O.M. and B.G., and ERC Starting Grant to O.M. The authors express gratitude to B. Morgenstern for expert help in editing this manuscript. B.G. holds the Erwin Neter Professorial Chair in Cell and Tumor Biology.

References

Al-Amoudi, A., Chang, J.J., Leforestier, A., McDowall, A., Salamin, L.M., Norlen, L.P., Richter, K., Blanc, N.S., Studer, D., Dubochet, J., 2004. Cryo-electron microscopy of vitreous sections. EMBO J. 23, 3583–3588.

Al-Amoudi, A., Studer, D., Dubochet, J., 2005. Cutting artefacts and cutting process in vitreous sections for cryo-electron microscopy. J. Struct. Biol. 150, 109–121.

Al-Amoudi, A., Diez, D.C., Betts, M.J., Frangakis, A.S., 2007. The molecular architecture of cadherins in native epidermal desmosomes. Nature 450, 832–837.

Al-Amoudi, A., Castano-Diez, D., Devos, D.P., Russell, R.B., Johnson, G.T., Frangakis, A.S., 2011. The three-dimensional molecular structure of the desmosomal plaque. Proc. Natl. Acad. Sci. USA 108, 6480–6485.

Bond, M., Somlyo, A.V., 1982. Dense bodies and actin polarity in vertebrate smooth muscle. J. Cell Biol. 95, 403–413.

Bouchet-Marquis, C., Hoenger, A., 2011. Cryo-electron tomography on vitrified sections: a critical analysis of benefits and limitations for structural cell biology. Micron 42, 152–162.

Chang, W.J., Ying, Y.S., Rothberg, K.G., Hooper, N.M., Turner, A.J., Gambliel, H.A., De Gunzburg, J., Mumby, S.M., Gilman, A.G., Anderson, R.G., 1994. Purification and characterization of smooth muscle cell caveolae. J. Cell Biol. 126, 127–138.

Christensen, A.K., 1971. Frozen thin sections of fresh tissue for electron microscopy, with a description of pancreas and liver. J. Cell Biol. 51, 772–804.

Delva, E., Tucker, D.K., Kowalczyk, A.P., 2009. The desmosome. Cold Spring Harb. Perspect Biol. 1, a002543.

Frank, J., Cserhalmi-Friedman, P.B., Ahmad, W., Panteleyev, A.A., Aita, V.M., Christiano, A.M., 2001. Characterization of the desmosomal cadherin gene family: genomic organization of two desmoglein genes on human chromosome 18q12. Exp. Dermatol. 10, 90–94.

Franke, W.W., Cowin, P., Schmelz, M., Kapprell, H.P., 1987. The desmosomal plaque and the cytoskeleton. Ciba Found. Symp. 125, 26–48.

Gabella, G., 1985. Chicken gizzard. The muscle, the tendon and their attachment. Anat. Embryol. (Berl.) 171, 151–162.

Garrod, D.R., 1993. Desmosomes and hemidesmosomes. Curr. Opin. Cell Biol. 5, 30–40.

Garrod, D., Chidgey, M., 2008. Desmosome structure, composition and function. Biochim. Biophys. Acta 1778, 572–587.

Garrod, D.R., Merritt, A.J., Nie, Z., 2002. Desmosomal adhesion: structural basis, molecular mechanism and regulation (review). Mol. Membr. Biol. 19, 81–94.

Geiger, B., Tokuyasu, K.T., Dutton, A.H., Singer, S.J., 1980. Vinculin, an intracellular protein localized at specialized sites where microfilament bundles terminate at cell membranes. Proc. Natl. Acad. Sci. USA 77, 4127–4131.

Geiger, B., Dutton, A.H., Tokuyasu, K.T., Singer, S.J., 1981. Immunoelectron microscope studies of membrane-microfilament interactions: distributions of alpha-actinin, tropomyosin, and vinculin in intestinal epithelial brush border and chicken gizzard smooth muscle cells. J. Cell Biol. 91, 614–628.

Giudice, G.J., Cohen, S.M., Patel, N.H., Steinberg, M.S., 1984. Immunological comparison of desmosomal components from several bovine tissues. J. Cell. Biochem. 26, 35–45.

Gruska, M., Medalia, O., Baumeister, W., Leis, A., 2008. Electron tomography of vitreous sections from cultured mammalian cells. J. Struct. Biol. 161, 384–392.

Gunst, S.J., Zhang, W., 2008. Actin cytoskeletal dynamics in smooth muscle: a new paradigm for the regulation of smooth muscle contraction. Am. J. Physiol. Cell Physiol. 295, C576–587.

Han, H.M., Zuber, B., Dubochet, J., 2008. Compression and crevasses in vitreous sections under different cutting conditions. J. Microsc. 230, 167–171.

Hanson, J.a.L.J., 1963. The structure of F-actin and of actin filaments isolated from muscle. J. Mol. Biol. 6, 46–60.

Hsieh, C.E., Marko, M., Frank, J., Mannella, C.A., 2002. Electron tomographic analysis of frozen-hydrated tissue sections. J. Struct. Biol. 138, 63–73.

Hsieh, C.-E., Leith, A., Mannella, C.A., Frank, J., Marko, M., 2006. Towards high-resolution three-dimensional imaging of native mammalian tissue: electron tomography of frozen-hydrated rat liver sections. J. Struct. Biol. 153, 1–13.

Kellenberger, E., Kistler, J., 1979. The physics of specimen preparation. In: Mason, H. (Ed.), Structure Research, vol. VII. FriedrVieweg & Son, Wiesbaden, pp. 1–14 (figure).

Koulu, L., Kusumi, A., Steinberg, M.S., Klaus-Kovtun, V., Stanley, J.R., 1984. Human autoantibodies against a desmosomal core protein in pemphigus foliaceus. J. Exp. Med. 160, 1509–1518.

Lucic, V., Leis, A., Baumeister, W., 2008. Cryo-electron tomography of cells: connecting structure and function. Histochem. Cell Biol. 130, 185–196.

Mader, A., Elad, N., Medalia, O., 2010. Cryoelectron tomography of eukaryotic cells. Methods Enzymol. 483, 245–265.

Marko, M., Hsieh, C., Schalek, R., Frank, J., Mannella, C., 2007. Focused-ion-beam thinning of frozen-hydrated biological specimens for cryo-electron microscopy. Nat. Methods 4, 215–217.

McDowall, A.W., Chang, J.J., Freeman, R., Lepault, J., Walter, C.A., Dubochet, J., 1983. Electron microscopy of frozen hydrated sections of vitreous ice and vitrified biological samples. J. Microsc. 131, 1–9.

Medalia, O., Weber, I., Frangakis, A.S., Nicastro, D., Gerisch, G., Baumeister, W., 2002. Macromolecular architecture in eukaryotic cells visualized by cryoelectron tomography. Science 298, 1209–1213.

Mollenhauer, H.H., 1993. Artifacts caused by dehydration and epoxy embedding in transmission electron microscopy. Microsc. Res. Tech. 26, 496–512.

Nickell, S., Forster, F., Linaroudis, A., Net, W.D., Beck, F., Hegerl, R., Baumeister, W., Plitzko, J.M., 2005. TOM software toolbox: acquisition and analysis for electron tomography. J. Struct. Biol. 149, 227–234.

Norlen, L., Oktem, O., Skoglund, U., 2009. Molecular cryo-electron tomography of vitreous tissue sections: current challenges. J. Microsc. 235, 293–307.

North, A.J., Gimona, M., Lando, Z., Small, J.V., 1994. Actin isoform compartments in chicken gizzard smooth muscle cells. J. Cell Sci. 107 (Pt 3), 445–455.

Patla, I., Volberg, T., Elad, N., Hirschfeld-Warneken, V., Grashoff, C., Fassler, R., Spatz, J.P., Geiger, B., Medalia, O., 2010. Dissecting the molecular architecture of integrin adhesion sites by cryo-electron tomography. Nat. Cell Biol. 12, 909–915.

Rigort, A., Bauerlein, F.J., Leis, A., Gruska, M., Hoffmann, C., Laugks, T., Bohm, U., Eibauer, M., Gnaegi, H., Baumeister, W., Plitzko, J.M., 2010. Micromachining tools and correlative approaches for cellular cryo-electron tomography. J. Struct. Biol. 172, 169–179.

Runswick, S.K., O'Hare, M.J., Jones, L., Streuli, C.H., Garrod, D.R., 2001. Desmosomal adhesion regulates epithelial morphogenesis and cell positioning. Nat. Cell Biol. 3, 823–830.

Sabanay, I., Arad, T., Weiner, S., Geiger, B., 1991. Study of vitrified, unstained frozen tissue sections by cryoimmunoelectron microscopy. J. Cell Sci. 100 (Pt 1), 227–236.

Sader, K., Studer, D., Zuber, B., Gnaegi, H., Trinick, J., 2009. Preservation of high resolution protein structure by cryo-electron microscopy of vitreous sections. Ultramicroscopy 110, 43–47.

Shao, Z., Shi, D., Somlyo, A.V., 2000. Cryoatomic force microscopy of filamentous actin. Biophys. J. 78, 950–958.

Shi, D., Somlyo, A.V., Somlyo, A.P., Shao, Z., 2001. Visualizing filamentous actin on lipid bilayers by atomic force microscopy in solution. J. Microsc. 201, 377–382.

Small, J.V., Gimona, M., 1998. The cytoskeleton of the vertebrate smooth muscle cell. Acta Physiol. Scand. 164, 341–348.

Small, J.V., Kaverina, I., 2003. Microtubules meet substrate adhesions to arrange cell polarity. Curr. Opin. Cell Biol. 15, 40–47.

Somlyo, A.P., 1985. Excitation–contraction coupling and the ultrastructure of smooth muscle. Circ. Res. 57, 497–507.

Somlyo, A.P., Somlyo, A.V., Kitazawa, T., Bond, M., Shuman, H., Kowarski, D., 1983. Ultrastructure, function and composition of smooth muscle. Ann. Biomed. Eng. 11, 579–588.

Steere, R.L., 1957. Electron microscopy of structural detail in frozen biological specimens. J. Biophys. Biochem. Cytol. 3, 45–60.

Steinberg, M.S., Shida, H., Giudice, G.J., Shida, M., Patel, N.H., Blaschuk, O.W., 1987. On the molecular organization, diversity and functions of desmosomal proteins. Ciba Found. Symp. 125, 3–25.

Tokuyasu, K.T., 1973. A technique for ultracryotomy of cell suspensions and tissues. J. Cell Biol. 57, 551–565.

Urban, E., Jacob, S., Nemethova, M., Resch, G.P., Small, J.V., 2010. Electron tomography reveals unbranched networks of actin filaments in lamellipodia. Nat. Cell Biol. 12, 429–435.

Wolfenson, H., Henis, Y.I., Geiger, B., Bershadsky, A.D., 2009. The heel and toe of the cell's foot: a multifaceted approach for understanding the structure and dynamics of focal adhesions. Cell Motil. Cytoskeleton 66, 1017–1029.

Yahav, T., Maimon, T., Grossman, E., Dahan, I., Medalia, O., 2011. Cryo-electron tomography: gaining insight into cellular processes by structural approaches. Curr. Opin. Struct. Biol. 21, 670–677.